Journal of Pharmaceutical Analysis 13 (2023) 1496–1509

Contents lists available at ScienceDirect

Journal of Pharmaceutical Analysis

journal homepage: www.elsevier.com/locate/jpa

Original article

Integrated mass spectrometry imaging reveals spatial-metabolic alteration in diabetic cardiomyopathy and the intervention effects of ferulic acid

Yanhua Liu [a, b], Xin Zhang [a, b], Shu Yang [a, b], Zhi Zhou [a, b], Lu Tian [c], Wanfang Li [c], Jinfeng Wei [c], Zeper Abliz [a, b, d, **], Zhonghua Wang [a, b, d, *]

[a] Key Laboratory of Mass Spectrometry Imaging and Metabolomics (Minzu University of China), National Ethnic Affairs Commission, Beijing, 100081, China
[b] Center for Imaging and Systems Biology, College of Life and Environmental Sciences, Minzu University of China, Beijing, 100081, China
[c] New Drug Safety Evaluation Center, Institute of Materia Medica, Peking Union Medical College, Beijing, 100050, China
[d] Key Laboratory of Ethnomedicine of Ministry of Education, School of Pharmacy, Minzu University of China, Beijing, 100081, China

ARTICLE INFO

Article history:
Received 30 May 2023
Received in revised form
28 July 2023
Accepted 10 August 2023
Available online 17 August 2023

Keywords:
Mass spectrometry imaging
Diabetic cardiomyopathy
Metabolic reprogramming
Ferulic acid

ABSTRACT

Diabetic cardiomyopathy (DCM) is a metabolic disease and a leading cause of heart failure among people with diabetes. Mass spectrometry imaging (MSI) is a versatile technique capable of combining the molecular specificity of mass spectrometry (MS) with the spatial information of imaging. In this study, we used MSI to visualize metabolites in the rat heart with high spatial resolution and sensitivity. We optimized the air flow-assisted desorption electrospray ionization (AFADESI)-MSI platform to detect a wide range of metabolites, and then used matrix-assisted laser desorption ionization (MALDI)-MSI for increasing metabolic coverage and improving localization resolution. AFADESI-MSI detected 214 and 149 metabolites in positive and negative analyses of rat heart sections, respectively, while MALDI-MSI detected 61 metabolites in negative analysis. Our study revealed the heterogenous metabolic profile of the heart in a DCM model, with over 105 region-specific changes in the levels of a wide range of metabolite classes, including carbohydrates, amino acids, nucleotides, and their derivatives, fatty acids, glycerol phospholipids, carnitines, and metal ions. The repeated oral administration of ferulic acid during 20 weeks significantly improved most of the metabolic disorders in the DCM model. Our findings provide novel insights into the molecular mechanisms underlying DCM and the potential of ferulic acid as a therapeutic agent for treating this condition.

1. Introduction

Diabetic cardiomyopathy (DCM) is leading cause of death in patients with chronic diabetes, accounting for over 70% of deaths due to cardiovascular complications or myocardial infarction [1,2]. Only in 2021, about 6.7 million people aged between 20 and 79 years died from diabetes and its complications. However, despite its prevalence, the underlying molecular mechanisms of DCM are not yet fully understood, and current treatments are limited [3–5].

Metabolites play essential roles in many cellular processes in the heart, including energy production, redox balance, signaling, and gene expression [6]. The concentration of metabolites in different heart regions may be associated with both normal and pathological processes. For instance, adenosine triphosphate (ATP) and creatine phosphate levels vary among different regions of the heart, reflecting their respective energy demands. The changes in the levels of amino acids, such as glutamate and taurine, can also affect the contractile function of cardiomyocytes. The distribution of metabolites in the heart is a dynamic process influenced by diverse factors such as age, diet, exercise, and diseases [7]. The alterations in metabolite distribution are indicators of impaired energy metabolism and oxidative stress in heart failure, myocardial infarction, and DCM [5,8]. Therefore, identifying metabolic

Peer review under responsibility of Xi'an Jiaotong University.
* Corresponding author. Key Laboratory of Mass Spectrometry Imaging and Metabolomics (Minzu University of China), National Ethnic Affairs Commission, Beijing, 100081, China.
** Corresponding author. Key Laboratory of Mass Spectrometry Imaging and Metabolomics (Minzu University of China), National Ethnic Affairs Commission, Beijing, 100081, China.
E-mail addresses: wangzhonghua@muc.edu.cn (Z. Wang), zeper@muc.edu.cn (Z. Abliz).

https://doi.org/10.1016/j.jpha.2023.08.011

biomarkers with spatial information is essential for understanding the mechanisms involved in heart diseases and developing effective diagnostic and therapeutic strategies.

Mass spectrometry imaging (MSI) is a powerful analytical technique that combines the molecular specificity of mass spectrometry (MS) with spatial imaging information, making it an ideal tool to identify and localize various known and unknown metabolites in tissue sections [9–11]. Since its introduction in 1997 by Caprioli et al. [12], MSI has undergone significant technological advancements, enabling its use in a wide range of biomedical applications. Currently, matrix-assisted laser desorption ionization (MALDI)-MSI and desorption electrospray ionization (DESI)-MSI are the two most frequently used MSI modalities, with each one having its unique advantages and disadvantages for imaging metabolites [13,14]. MALDI-MSI can achieve high-sensitivity and high-spatial resolution (up to 10 μm) imaging of certain metabolites by optimizing matrix deposition procedures. However, detecting a broad range of metabolites is challenging for MALDI-MSI due to matrix interference at less than *m/z* 500 [15,16]. DESI-MSI is a promising alternative to MALDI-MSI as it enables "the direct" detection of small molecules in tissue sections without requiring complicated matrix deposition processes [17,18]. Furthermore, ambient air-flow-assisted desorption electrospray ionization (AFADESI)-MSI offers high sensitivity and broad coverage, enabling simultaneous visualization thousands of metabolites in an untargeted analysis [19]. However, the spatial resolution of DESI-MSI and AFADESI-MSI is approximately 100 μm, limiting their use in high spatial resolution MSI analyses [20].

Although promising results have been obtained using MALDI-MSI and DESI-MSI, studies on metabolites in heart diseases using MSI are still in their early stages. Menger et al. [21] demonstrated the involvement of phospholipase A2 and arachidonic acid in acute myocardial infarction using MALDI-MSI. Similarly, Margulis et al. [22] identified metabolic signatures of myocardial infarction in mice by applying machine learning algorithms to DESI-MSI data. However, due to the vast number and structural diversity of metabolites, the MSI methods used in these studies offered a relatively limited metabolic coverage. Therefore, comprehensive MSI platforms are needed to provide a more detailed understanding of the molecular alterations in the heart following DCM and other metabolic heart diseases.

In this study, we reported the development of a sensitive, wide-coverage, and high spatial resolution MSI approach for mapping metabolites in the rat heart. The key parameters of the AFADESI-MSI platform were optimized to detect as many metabolites as possible. Additionally, MALDI-MSI was utilized to increase metabolic coverage and improve localization resolution. Our method revealed the metabolic heterogeneity and reprogramming of the heart in DCM model rats and the intervention effect of ferulic acid, an anti-myocardial injury drug candidate, on the metabolic landscape of the disease. The research strategy is depicted in Fig. 1.

2. Materials and methods

2.1. Chemicals and reagents

High-performance liquid chromatography (HPLC)-grade methanol (MeOH), acetonitrile (ACN), isopropanol (IPA), and ferulic acid were obtained from Fisher Scientific (Loughborough, UK). HCl was purchased from Sinopharm Chemical Reagent Co., Ltd. (Shanghai, China). Ferulic acid, 1,5-diaminonaphthalene (1,5-DAN), citrate, streptozotocin (STZ), and sodium carboxymethyl cellulose (Na-CMC) were provided by Sigma-Aldrich (St. Louis, MO, USA). Ultrapure water was purchased from Wahaha Co., Ltd. (Hangzhou, China).

2.2. Animal model

Six-week-old male Wistar rats weighing 180–200 g were procured from Vital River Laboratory Animal Technology Co., Ltd. (Beijing, China) and kept under a controlled 12 h light/dark cycle with constant temperature (20–26 °C) and humidity (40%–70%). Rats were given food and water ad libitum. The animals were randomly divided into two groups, i.e., the control group ($n = 8$) and the model group ($n = 24$), and received normal and high-fat diets, respectively. After four weeks, the model group received a single intraperitoneal injection of STZ (35 mg/kg body weight), while rats of the control group received freshly prepared citrate buffer (0.1 mol/L, pH 4.4, vehicle). The fasting blood glucose (FBG) concentrations were measured 5–7 days after administration, and rats having FBG levels greater than 16.7 mmol/L for three consecutive days were considered diabetic and selected for further studies. The model group animals were randomly divided into three groups: DCM group ($n = 8$), low-dose ferulic acid group (L-ferulic acid, $n = 8$), and high-dose ferulic acid group (H-ferulic acid, $n = 8$). Rats of the L-ferulic acid and H-ferulic acid groups received intragastric administration of ferulic acid once a day at doses of 50 and 200 mg/kg, respectively. Given its established efficiency for mitigating oxidative stress and inflammation in various animal models, the administration of ferulic acid at a dose of 50 mg/kg was selected. A higher dose of 200 mg/kg was employed to investigate the dose-dependent effects of ferulic acid on DCM, as supported by its safety and effectiveness in prior studies [23–25]. The control group and model control group were treated with 0.5% Na-CMC (vehicle) at intragastric doses of 10 mL/kg body weight. The administration of the drug or vehicle continued for 20 weeks, and the general state of animals was observed daily, while body weight, food intake, and water intake were measured weekly. FBG levels were measured every two weeks. At the end of the administration period, blood samples from the abdominal aorta were collected for biochemical index detection. Subsequently, heart samples were harvested, weighed, fixed in liquid nitrogen, and stored at −80 °C. All animal experiments were conducted in accordance with the Guide for the Care and Use of Laboratory Animals and were approved by the Animal Welfare Ethics Committee of Beijing United-Genius Pharmaceutical Technology Development Co., Ltd. (Beijing, China) (Approval No.: TS19100-YX, 2 December 2019).

2.3. Biochemical analysis and histopathological staining

The alanine aminotransferase (ALT), aspartate aminotransferase, lactate dehydrogenase (LDH), creatine kinase (CK), glucose, and triglyceride (TG) levels in the blood were measured using the AU480 automatic chemical analyzer (Beckman Coulter Inc., Brea, CA, USA). The concentration of HbA1c was measured using the Quo Test HbA1c analyzer (QUOTIENT Diagnostics Ltd., Walton-on-Thames, UK).

The heart tissue was fixed in saline solution, embedded in a cryostat chuck, and then sectioned at a thickness of 10 μm using a cryostat (Leica CM1860, Microsystems Ltd., Wetzlar, Germany) at −20 °C. The horizontal short-axis section of the left ventricular papillary muscle was used for further analyses. The sections were mounted onto adhesive microscope slides, air-dried at room temperature, and stained with hematoxylin and eosin (H&E), and Masson dye. To analyze the histopathological damage, the stained heart tissue sections were scanned using a digital section scanner (Ningbo Jiangfeng Bioinformatics Co., Ltd., Ningbo, China). Masson staining images were analyzed using ImageJ software. Collagen volume fraction was obtained from ratio of the collagen tissue areas divided by the whole tissue area within the same microscopic field.

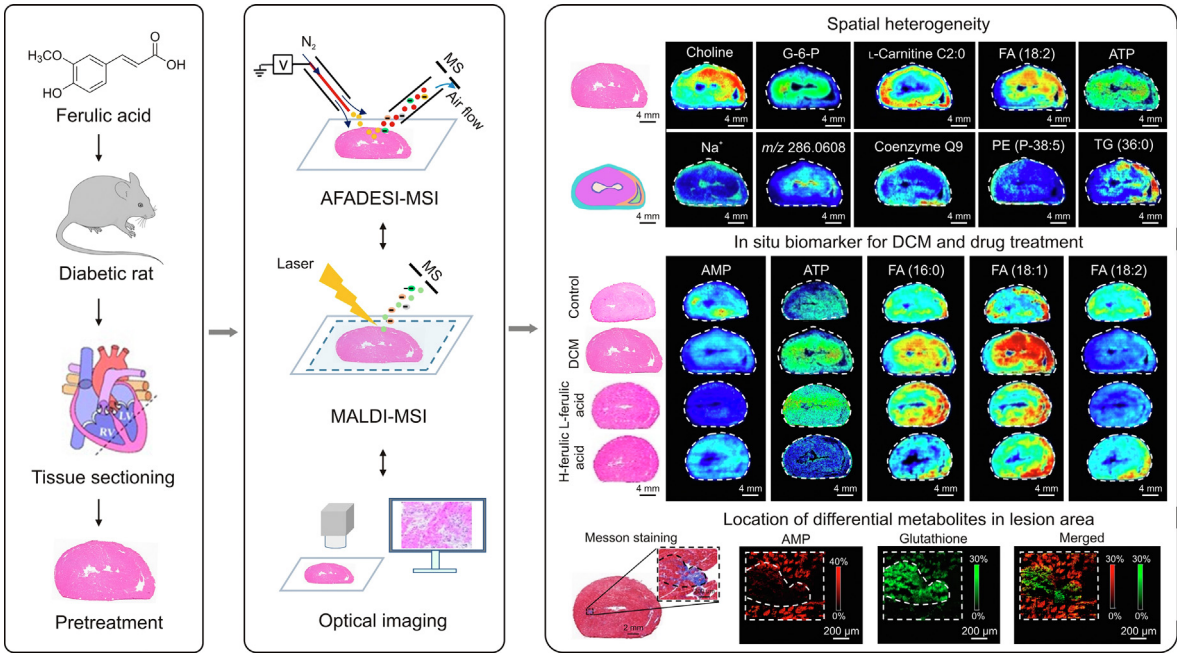

Fig. 1. Research scheme for spatial-resolved metabolic reprogramming in diabetic cardiomyopathy (DCM) using air flow-assisted desorption electrospray ionization (AFADESI) and matrix-assisted laser desorption ionization (MALDI) integrated mass spectrometry imaging (MSI). MS: mass spectrometry; G-6-P: glucose-6-phosphate; FA: fatty acid; ATP: adenosine triphosphate; PE: phosphatidylethanolamine; TG: triglyceriol; L-ferulic acid: low-dose ferulic acid (50 mg/kg); H-ferulic acid: high-dose ferulic acid (200 mg/kg); AMP: adenosine monophosphate; ATP: adenosine triphosphate.

2.4. Sample preparation for AFADESI- and MALDI-MSI analyses

The frozen heart tissues were sliced into sections with a thickness of 10 μm and mounted onto adhesive microscope slides and indium tin oxide (ITO) coated glass slides. The sections were then stored at −80 °C until analysis. Prior to AFADESI- and MALDI-MSI analysis, all sections were vacuum-dried for 30 min.

The MALDI matrix was sprayed directly onto the tissue surface using an automated spray device (TM-Sprayer, HTX Technologies, Carrboro, NC, USA). The matrix solution of 1,5-DAN hydrochloride and 2,5-dihydroxybenzoic acid was prepared according to the literature procedure [26]. The details of preparation steps of matrix and spraying parameters are provided in the Supplementary data.

2.5. AFADESI- and MALDI-MSI analyses of heart tissue sections

A laboratory-built AFADESI-MS platform consisting of an AFADESI ambient ion source and a Q-OT-qIT hybrid mass spectrometer (Orbitrap Fusion Lumos Thermo Fisher Scientific Inc., San Jose, CA, USA) was designed for AFADESI-MSI analysis. Mass data were acquired in positive and negative ionization modes with a scan range of 100−1,000 Da and mass resolution of 120,000 full width at half maximum (FWHM) at *m/z* 200. The capillary temperature was set at 350 °C, and the spray voltage was ±3 kV. A MeOH:H_2O (8:2, *V*/*V*) spray solvent was selected for the AFADESI-MSI analysis, and the flow rate was set to 7 μL/min. The pressure of the spray gas (N_2) was 0.6 MPa, and the extracting gas flow rate was 45 L/min. The heart tissue sections were scanned at a moving speed of 0.16 mm/s in the *x*-step, and the vertical *y*-step was 0.2 mm. The distance and angle between the sprayer and the tissue slice and between the sprayer and the transfer tube were adjusted to obtain highest signal intensity. Data were acquired using the Xcalibur software (Version 4.0, Thermo Scientific Inc.).

The MALDI-MSI experiments were conducted on an Autoflex Speed MALDI time-of-flight (TOF)/TOF mass spectrometer (Bruker Daltonics, Billerica, MA, USA) equipped with a 2,000-Hz solid-state Smartbeam Nd:YAG solid-state laser (λ = 355 nm) (Azura Laser AG, Berlin, Germany). Mass data were acquired in scanning mode from *m/z* 80−1,000 Da in negative ion reflection mode, with a spatial resolution of 50 μm. High-resolution MSI data were collected at a spatial resolution of 10 μm in positive and negative ion reflection modes. The laser spot size was set to "small", and the laser power was optimized at the beginning of each operation and then remained unchanged throughout the experiment. External standards were used for quality calibration before each data acquisition. Data acquisition was conducted using FlexAnalysis 3.4 and FlexImaging 4.1 software (Bruker Daltonics).

2.6. Data processing and analysis

AFADESI-MSI data were processed and analyzed by the procedure described below. First, original data files in .raw format were converted to .cdf files using Xcalibur software. Subsequently, files were imported into imaging software (MassImager 2.0, Beijing, China) to reconstruct the ion image. Next, the background image was subtracted, and regions of interest were manually drawn by matching H&E-stained images of adjacent heart slices. The average ion intensity of the marked area was then obtained, and two-dimensional data matrices were generated in .txt format (*m/z*, intensity). Data were imported to Markerview 1.2.1 (AB SCIEX, Toronto, Ontario, Canada) for background subtraction, peak extraction, and alignment. To ensure data reliability and reproducibility, only ions with intensity higher than 100 a.u. in at least 50% of the samples in one group were included in further analyses. The relative ion intensities were obtained by normalization using total ion current (TIC). The Student's *t*-test analysis was performed between the control group and the DCM group and between the model group and the ferulic acid-treated group, respectively, to identify differential metabolites associated with DCM and the therapeutic effect of ferulic acid. A statistically significant difference was defined as $P < 0.05$.

MALDI-MSI data were imported to SCiLS software 2016b (SCiLS, Bremen, Germany) for image reconstruction, peak extraction, and alignment. The resulting MS data were normalized using TIC to

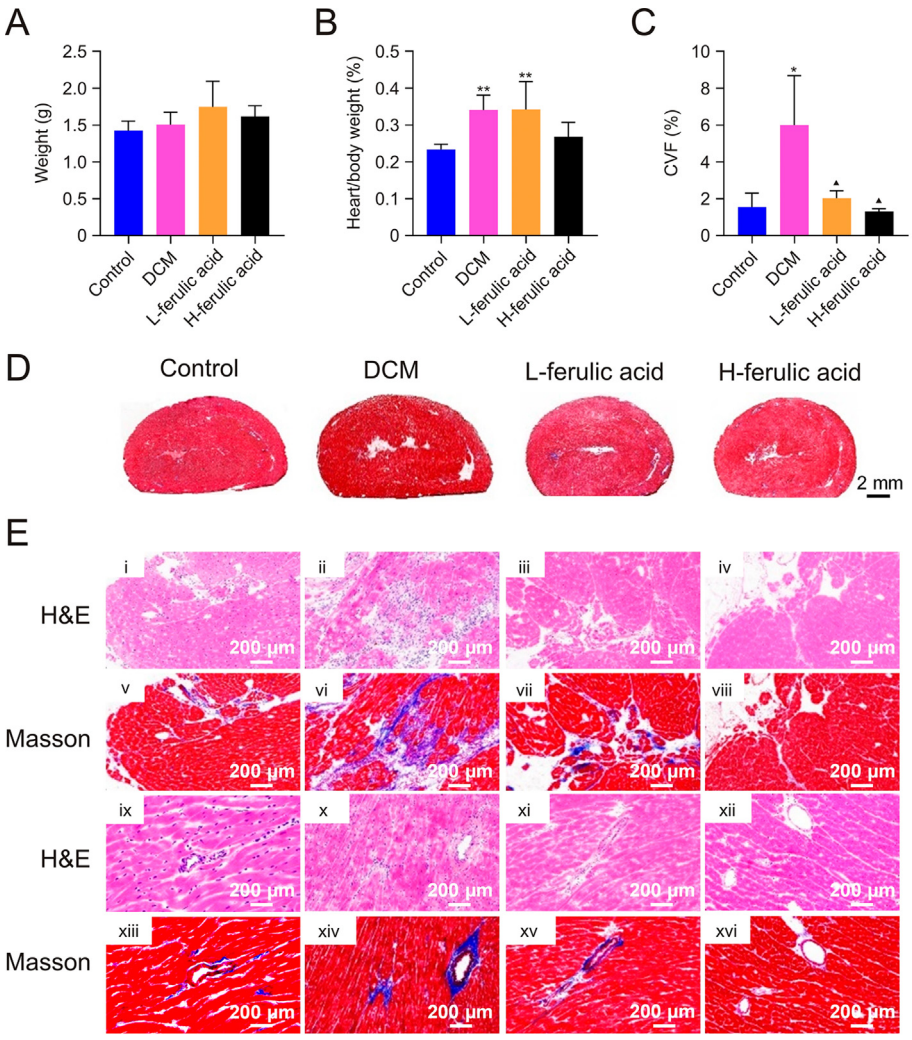

Fig. 2. The histogram of (A) heart weight, (B) heart/body weight ratio, (C) collagen volume fraction (CVF), (D) Masson staining images of whole heart sections, and (E) hematoxylin and eosin (H&E) and Masson staining images of 20-fold magnification in the control, diabetic cardiomyopathy (DCM), low-dose ferulic acid (50 mg/kg) (L-ferulic acid), and high-dose ferulic acid (200 mg/kg) (H-ferulic acid) groups. H&E staining images (i–iv) and Masson staining (v–viii) images of local cardiac tissue in the control, DCM, L-ferulic acid, and H-ferulic acid groups. H&E staining image (ix–xii) and Masson staining image (xiii–xvi) of heart perivascular tissue in control, DCM, L-ferulic acid, and H-ferulic acid groups. $^{*}P < 0.05$ and $^{**}P < 0.01$, as compared to the control group; $^{▲}P < 0.05$, as compared to the DCM group (mean ± standard deviation, $n = 8$).

obtain the relative intensity of ion signals in the region of interest. Statistical analysis was performed using the same methods as for the AFADESI-MSI analysis. A significance level of $P < 0.05$ was used for statistical tests.

2.7. Liquid chromatography (LC)-MS/MS analysis

The LC-MS/MS analysis of heart tissue homogenates was performed in positive and negative ionization modes with a Q-OT-qIT hybrid mass spectrometer (Orbitrap Fusion Lumos, Thermo Fisher Scientific Inc.) connected to an UltiMate 3000 series HPLC system (Thermo Fisher Scientific Inc.). The procedure for sample preparation and instrumental parameters for LC-MS/MS analysis are provided in the Supplementary data.

2.8. Metabolite identification

The identification of metabolites structures was performed according to previously described protocols [27,28]. Initially, possible element compositions for each ion were estimated using Xcalibur 4.0 (Thermo Fisher Scientific Inc.) based on its exact mass (expected mass accuracy < 5 ppm) and isotope patterns. These ions were then matched against The Human Metabolome Database (HMDB) (http://hmdb.ca/) [29], METLIN (http://metlin.scripps.edu/) [30], LIPID MAPS (www.lipidmaps.org) [31], and a home-made metabolite library [19] to find possible metabolites. The structures of metabolites were confirmed through high-resolution on-tissue AFADESI-MS/MS analysis performed on heart sections, as well as LC-MS/MS analysis of heart tissue homogenates.

3. Results and discussion

3.1. Physiological, biochemical, and histopathological analyses

We observed that the DCM group exhibited lower body weight and food intake and higher water intake than the control group (Fig. S1). As shown in Fig. S2, blood biochemical indicators revealed that glucose and HbA1c levels in the DCM group were significantly increased compared with the control group. TG, LDH, and CK levels were slightly increased, and ALT level was significantly increased in the DCM group. After treatment with ferulic acid, the H-ferulic acid

group exhibited a higher body weight and food intake and lower water intake than non-treated rats. Furthermore, the H-ferulic acid group showed a slight decrease in the blood levels of glucose, HbA1c, TG, ALT, and CK.

tAs shown in Fig. 2, the heart weight and heart-to-body weight ratio were significantly higher in the DCM group than in the control group. The histological examination of the heart tissues stained with H&E and Masson dye revealed pathological lesions including myocardial cells hypertrophy, inflammatory cells infiltration, myocardial fibrosis, and proliferation of extravascular collagen fibers in the DCM group. After treatment with ferulic acid, the heart-to-body weight ratio decreased significantly, and the heart histological lesions were ameliorated in the H-ferulic acid group.

The physiological, biochemical, and histopathological characteristics observed in rats of the DCM group are consistent with the clinical features of DCM, thereby evidencing that the animal model was successfully developed. Furthermore, our findings suggest that the treatment with high doses of ferulic acid has a beneficial effect on myocardial injury in diabetic animals.

3.2. Optimization of the AFADESI-MSI method

We optimized the AFADESI-MSI platform parameters to enhance the metabolites detection and obtain high-quality MS images. The spray solvent significantly affects metabolite desorption and ionization in biological tissues. We analyzed adjacent tissue sections from the same rat heart to investigate the effects of spray solvent composition and flow rate on sensitivity and spatial resolution. Five commonly used spray solvents, namely, MeOH:H_2O (8:2, *V*/*V*), MeOH:IPA:H_2O (4:4:2, *V*/*V*/*V*), ACN:H_2O (8:2, *V*/*V*), ACN:IPA:H_2O (4:4:2, *V*/*V*/*V*), and IPA:H_2O (8:2, *V*/*V*), were evaluated. Our results revealed that MeOH:H_2O (8:2, *V*/*V*) shows the highest ion response intensities and produces the optimal MS images (Figs. 3A and S3A). Next, flow rate of the spray solvent at 5 and 7 μL/min were compared. We found that a flow rate of 7 μL/min resulted in higher MS response intensities for most of the representative ions (Figs. 3B and S3B). Therefore, MeOH:H_2O (8:2, *V*/*V*) at 7 μL/min was selected for subsequent AFADESI-MSI analysis.

The scanning speed is another important parameter affecting sensitivity and spatial resolution in AFADESI-MSI analysis. We

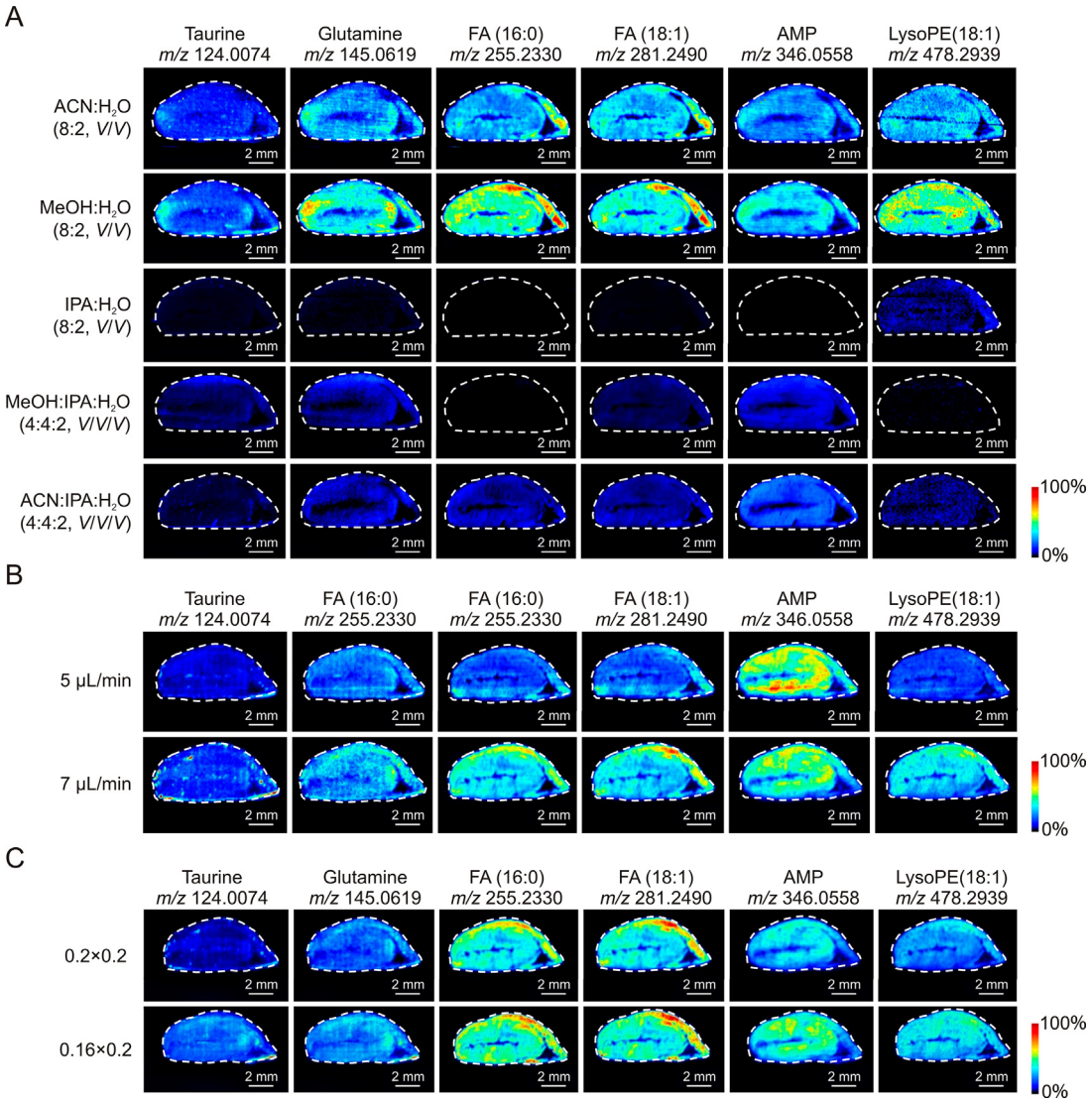

Fig. 3. Mass spectrometry images (MSIs) of representative metabolites total ion current intensity detected through the negative air flow-assisted desorption electrospray ionization (AFADESI)-MSI analysis of consecutive heart tissue sections using different (A) spray solvent compositions, (B) flow rate of spray solvent, and (C) scanning speed of spray solvent. ACN: acetonitrile; MeOH: methanol; IPA: isopropanol; FA: fatty acid; AMP: adenosine monophosphate; LysoPE: lysophosphatidylethanolamine.

compared the scanning rate of 0.16 and 0.2 mm/s in the *x*-direction, and found that a canning rate of 0.16 mm/s produced higher MS response intensities and better MS images (Figs. 3C and S3C). Other parameters of the AFADESI-MSI platform were set to provide optimal response to endogenous metabolites in heart tissues, based on our previous work [27].

3.3. AFADESI-MSI and MALDI-MSI analyses

The heart is highly heterogeneous organ and can be subdivided into various regions according to anatomical structure, cellular composition, and physiological function. In this study, we transversely sectioned rat hearts at the ventricular level to expose the left and right ventricles as distinct chambers (Fig. 4). AFADESI-MSI and MALDI-MSI analyses of heart sections in control, DCM, L-ferulic acid, and H-ferulic acid groups were performed. The positive and negative AFADESI-MS analyses of heart sections detected 2,061 and 1,216 ion features, respectively, from which we putatively identified 214 and 159 metabolites (Tables S1 and S2). Additionally, the negative MALDI-MS analysis detected 177 ion features, from which 60 metabolites were putatively identified (Table S3).

Our results show that these metabolites exhibited a heterogeneous distribution across the heart sections (Fig. 4). Choline, for example, exhibited abundant distribution across sections, showing the highest density in the right ventricle. L-carnitine, creatine, glucose-6-phosphate (G-6-P), adenosine diphosphate (ADP), and ATP were mainly distributed in the myocardium of the left ventricle. Moreover, L-carnitine C16:1, phosphocholine (PC (36:2)), linoleic acid (FA (18:2)), lysophosphatidylethanolamine (LysoPE (18:2)), glutathione (GSH), ascorbic acid, inosine monophosphate (IMP), and PE (38:1) were abundantly distributed in the myocardium of both the right and left ventricles. In contrast, L-carnitine 2:0, coenzyme Q9, inosine, LysoPE (22:4), and PE (40:6) showed higher concentrations in the outer layer of the heart. An unknown metabolite with *m/z* 286.0608 was mostly distributed in the endomyocardium. Interestingly, glycerides such as monoacylglycerol (MG (18:1)), diacylglycerol (DG (36:2), DG (36:1-O)), and TG (36:0) accumulated in the right ventricle, while phosphatidylinositol (PI (38:4)) and PE (P-38:5) were mainly concentrated in the outer layer of the right ventricle. Additionally, glucose, Na^+, and K^+ were mainly present in the residual blood in the ventricular cavity. These findings reveal substantial spatial heterogeneity in the metabolic activity within the heart, and the non-uniform distribution of these metabolites suggests that they may play a role in maintaining distinctive structural and functional characteristics of heart regions. Furthermore, these metabolites could be used as specific structure markers to guide the investigation of local metabolic activity in the heart.

To identify metabolites involved in DCM, a comparison of local metabolic profiles was performed between the heart tissues of the control and DCM groups. Using an independent Student's *t*-test with $P < 0.05$, we identified 24 differential metabolites in the positive AFADESI-MSI analysis and 60 differential metabolites in the negative AFADESI-MSI analysis (Tables S4 and S5). Additionally, we identified 35 discriminating metabolites in the negative MALDI-MSI analysis, and 14 of them were consistent with those identified by the AFADESI-MS analysis, including ascorbic acid, glucose, ribose-5-phosphate (R-5-P), G-6-P, glutamine, palmitic acid (FA (16:0)), stearic acid (FA (18:0)), oleic acid (FA (18:1)), FA (18:2), arachidonic acid (FA (20:4)), PE (38:6), PE (38:5), PE (40:6), and phosphatidylserine (PS (40:6)) (Table S6). The multiple alterations in these specific metabolites are shown in Fig. S4.

High spatial resolution (10 μm) MALDI-MSI guided by Masson's staining was performed to determine the specific distribution of differential metabolites identified by AFADESI- and MALDI-MSI analyses in pathological micro-regions. The levels of these metabolites were significantly different between normal and diseased areas of the myocardial tissue characterized by collagen fiber accumulation, as shown in Fig. 5. For instance, GSH (*m/z* 306.0752) was mainly observed in the lesion area (Fig. 5C), while adenosine monophosphate (AMP, *m/z* 346.0552) was predominantly present in the non-lesion area (Fig. 5B). Additionally, we noted significant accumulation of Na^+, taurine, glutamine, glucose, inosine, choline, PC (34:2), and PC (36:2) in the lesion area compared to the non-lesion area. These findings provide further insights into the role of these metabolites in the pathogenesis of DCM.

3.4. Spatial-metabolic alterations in DCM

The discriminating metabolites associated with DCM spanned a range of metabolite classes, including carbohydrates, amino acids, organic acids, nucleotides and their derivatives, choline, polyamines, carnitine, fatty acids and their derivatives, phosphate compounds, metal ions, and vitamins. This diversity suggests that significant changes in the metabolic profile occur in the hearts of diabetic rats. To gain insight into the metabolic pathways involved in DCM, we performed metabolic pathway enrichment analysis using MetaboAnalyst 4.0. As shown in Fig. S5, we identified 27 metabolic pathways closely related to DCM with an impact value > 0.

The spatial distribution and changes of the metabolites involved in glucose metabolism are shown in Figs. 6 and S6. The myocardium has a high energy demand due to the continuous rhythmic cardiac contraction and relaxation [32]. Studies have shown that the human heart consumes the most energy per gram of tissue compared to other organs, utilizing approximately 6 kg of ATP per day, which is about 20 times its own weight [33,34]. Under normal physiological conditions, approximately 95% of the total energy generated by the heart is through mitochondrial oxidative phosphorylation of fatty acids and glucose. In this study, glucose levels were significantly decreased in the hearts of diabetic rats, especially in the left ventricular myocardium. In addition, intermediate metabolites involved in glucose metabolism, such as G-6-P, glyceraldehyde-3-phosphate (G-3-P), and R-5-P, were also decreased in the diabetic heart. These results could potentially be related to the impaired glucose uptake in the heart in the diabetic state, which might be a consequence of insulin resistance or impaired insulin signaling pathways.

Multiple metabolites involved in the tricarboxylic acid (TCA) cycle were found changed significantly in the DCM group (Figs. 6 and S6). Compared to the control group, the DCM group exhibited significantly reduced levels of succinic acid, malic acid, glutamate, and glutamine in the heart. Succinic acid and malic acid are intermediates of the TCA cycle and are crucial for energy production. Succinic acid is a substrate of succinate dehydrogenase (SDH), an enzyme involved in the mitochondrial electron transfer chain [35,36]. Additionally, succinic acid exhibits antioxidant properties and protects the heart against oxidative stress-induced damage [37]. Therefore, the decrease in the levels of succinic acid and malic acid in the DCM group indicates altered SDH activity and mitochondrial dysfunction in diabetic rat heart, which could lead to insufficient ATP production and impaired cardiac function. Glutamate is an amino acid that can be synthesized from alpha-ketoglutarate, an intermediate of the TCA cycle [38]. Glutamine is an amino acid synthesized from glutamate. Glutamate and glutamine play a role in the generation of nitric oxide, which can modulate the autonomic nervous system and influence heart rate and contractility [39,40]. Decreased levels of glutamate and glutamine have been associated with various cardiovascular diseases, such as heart failure and myocardial infarction.

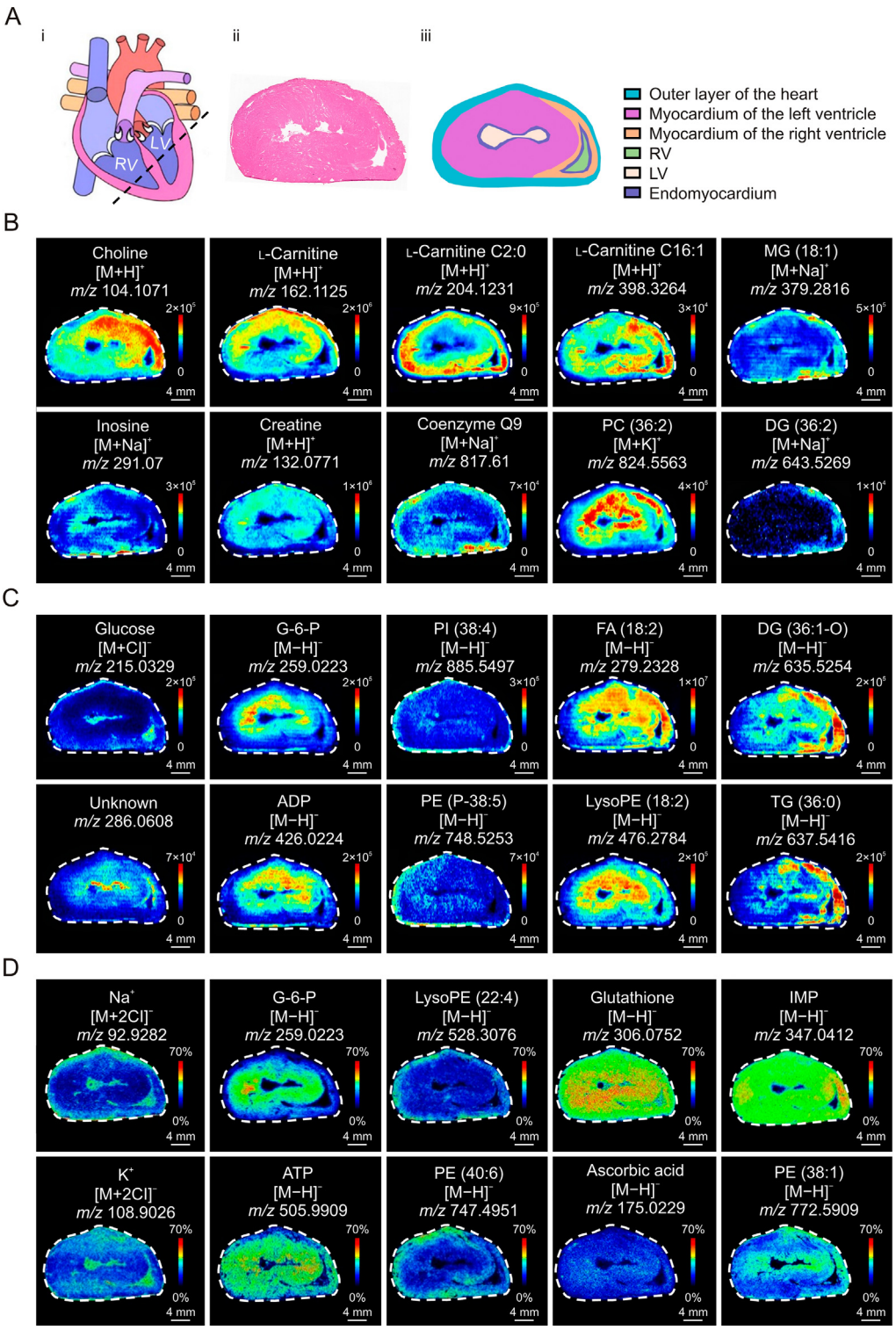

Fig. 4. Ion images of representative metabolite ions in positive and negative modes in air flow-assisted desorption electrospray ionization (AFADESI)- and matrix-assisted laser desorption ionization (MALDI)-mass spectrometry imaging (MSI). (A) Structure diagram of rat heart: transverse section (i), hematoxylin and eosin (H&E) stain (ii), and structure diagram of rat heart (iii). (B, C) Ion images of representative metabolite ions in positive (B) and negative (C) modes in AFADESI-MSI. (D) Ion images of representative metabolite ions in negative modes in MALDI-MSI. RV: right ventricle; LV: left ventricle. MG: monoacylglycerol; PC: phosphocholine; DG: diacylglycerol; G-6-P: glucose-6-phosphate; PI: phosphatidylinositol; FA: fatty acid; ADP: adenosine diphosphate; PE: phosphatidylethanolamine; LysoPE: lysophosphatidylethanolamine; TG: triglyceriol; IMP: inosine monophosphate; ATP: adenosine triphosphate.

We observed that fatty acid metabolism in the DCM group was significantly different when compared to the normal group (Figs. 7, S7, and S8). A significant accumulation of long-chain saturated and monounsaturated fatty acids such as FA (16:0), FA (18:0), arachidic acid (FA (20:0)), behenic acid (FA (22:0)), lignoceric acid (FA (24:0)), and FA (18:1) was observed in heart tissues of diabetic rats, particularly in the myocardium. This is consistent with the fact that uptake and utilization of glucose by myocardial

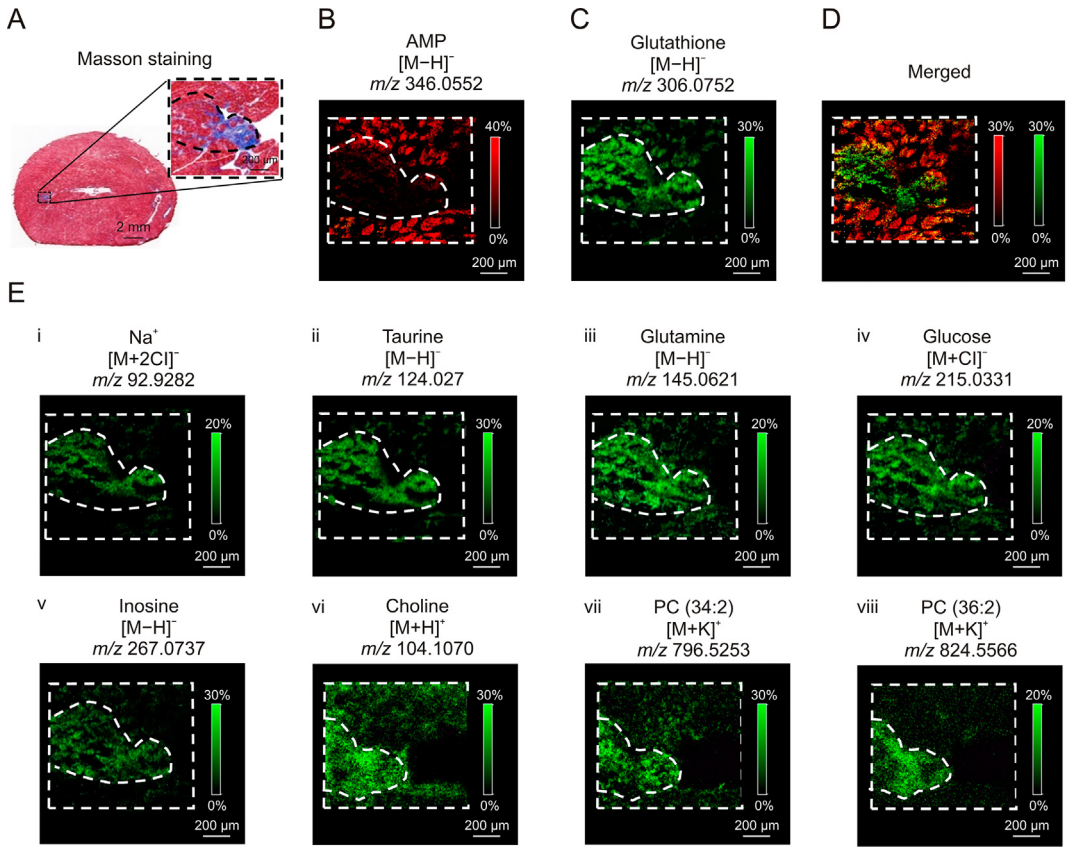

Fig. 5. High-resolution matrix-assisted laser desorption ionization (MALDI)-mass spectrometry imaging (MSI) image of lesion micro-area. (A) Masson staining image of heart tissue section. (B–D) Ion images of adenosine monophosphate (AMP) at *m/z* 346.0552 (B), glutathione (GSH) at *m/z* 306.0752 (C), and merged image (D). (E) Ion image of Na^+ at *m/z* 92.9282 (i), taurine at *m/z* 124.027 (ii), glutamine at *m/z* 145.0621 (iii), glucose at *m/z* 215.0331 (iv), inosine at *m/z* 267.0737 (v), choline at *m/z* 104.1070 (vi), phosphocholine (PC (34:2)) at *m/z* 796.5253 (vii), and PC (36:2) at *m/z* 824.5566 (viii).

cells is limited in diabetes, which forces the heart to rely on other sources of energy, such as fatty acids. The fatty acids detected in this study are the most abundant in the human body and serve as the primary energy source to meet the high energy demands of the heart. However, fatty acids accumulation may be associated with detrimental health effects (e.g., inflammation, insulin resistance, and oxidative stress), contributing to cardiac dysfunction [41–43].

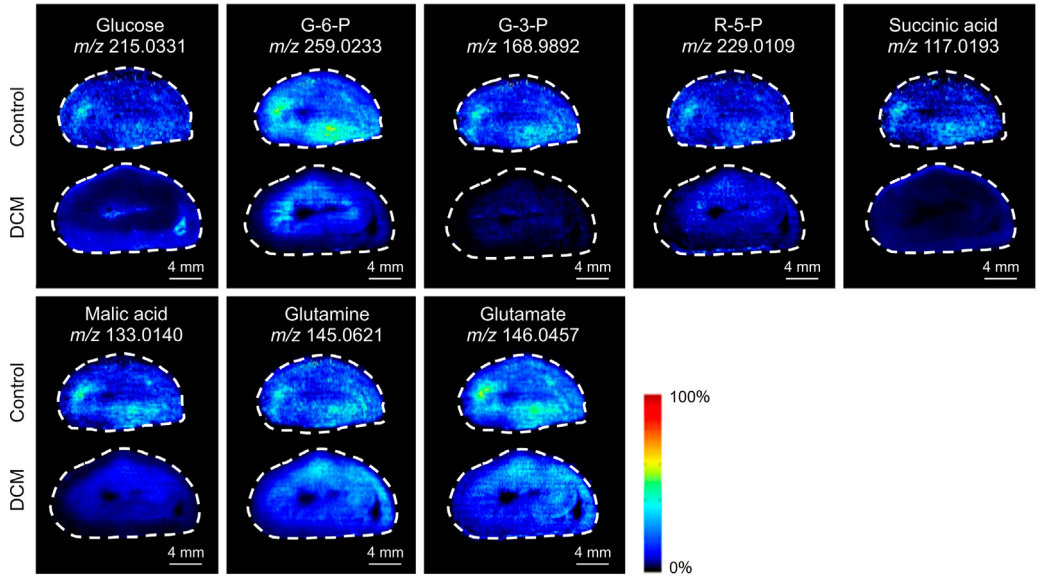

Fig. 6. Ion images of mass spectrometry imaging (MSI) analysis of metabolites involved in glucose metabolism pathways in the heart in the control and diabetic cardiomyopathy (DCM) groups. G-6-P: glucose-6-phosphate; G-3-P: glyceraldehyde-3-phosphate; R-5-P: ribose-5-phosphate.

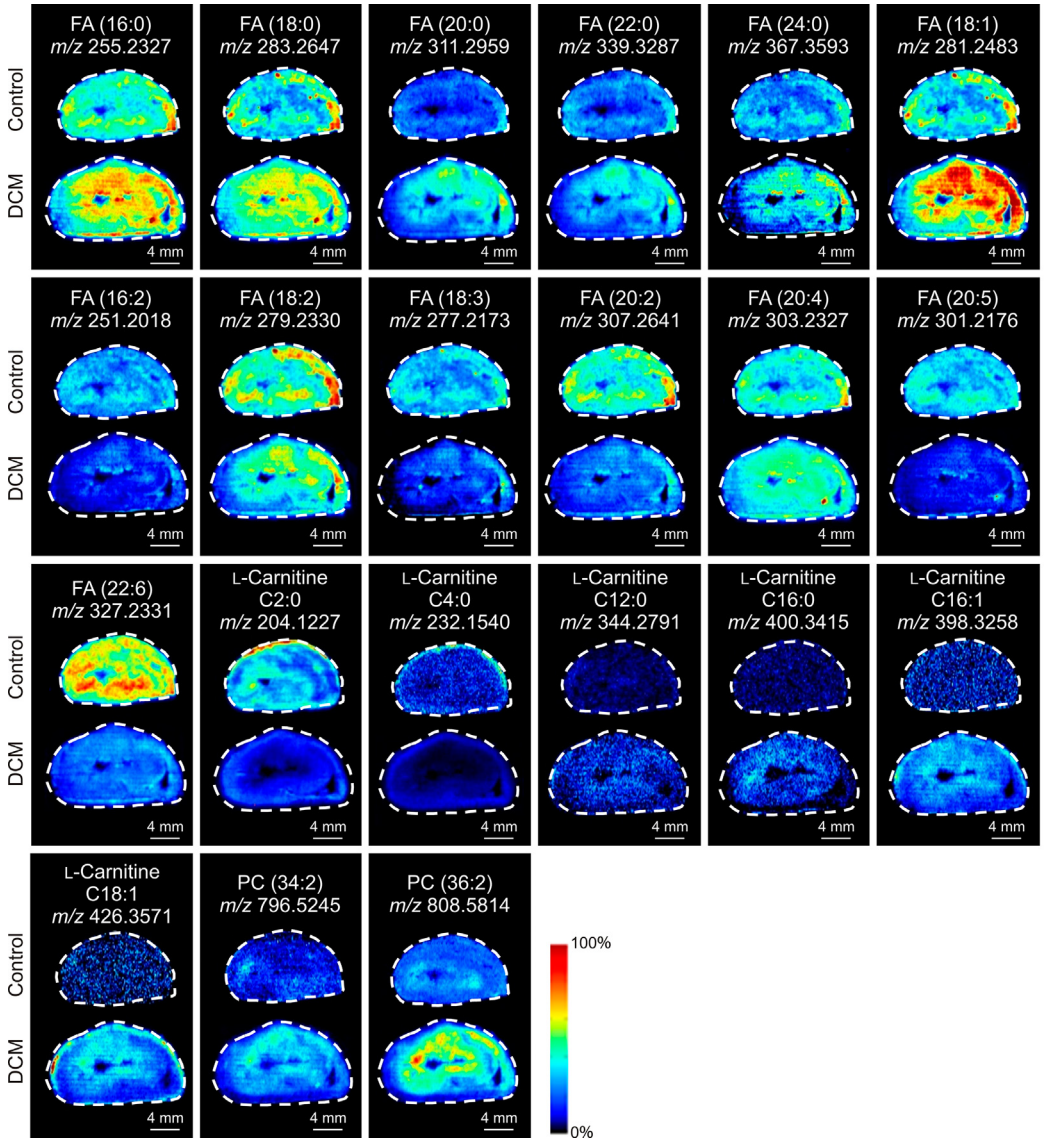

Fig. 7. Ion images of air flow-assisted desorption electrospray ionization (AFADESI)-mass spectrometry imaging (MSI) analysis of metabolites involved in lipid metabolism in the heart in rats of the control and diabetic cardiomyopathy (DCM) groups. FA: fatty acid; PC: phosphatidylcholine.

In contrast to long-chain saturated and monounsaturated fatty acids, seven polyunsaturated fatty acids (PUFAs) including hexadecadienoic acid (FA (16:2)), FA (18:2), linolenic acid (FA (18:3)), eicosadienoic acid (FA (20:2)), arachidonic acid (FA (20:4)), eicosapentaenoic acid (FA (20:5)), and docosahexaenoic acid (FA (22:6)) in heart sections of diabetic rats were significantly lower than in normal control rats. PUFAs are crucial for maintaining membrane fluidity and regulating cardiac inflammation [44,45]. In diabetes, the enzymes and metabolic pathways involved in PUFA synthesis can be impaired, reducing the conversion of precursor fatty acids into PUFAs. Furthermore, oxidative stress and inflammation in diabetes can alter the enzymes required for converting precursor fatty acids into PUFAs. Given the role of PUFAs in regulating cardiac inflammation, it is unsurprising that their down-regulation has been associated with cardiovascular disease [46].

Our study showed that the fatty acyl-carnitine metabolism in the DCM group was significantly different when compared to the normal group (Figs. 7 and S7). Short-chain acyl carnitines, including L-carnitine C2:0 and L-carnitine C4:0, was significantly lower in the DCM group than in the control group. In contrast, long-chain acyl carnitines, including L-carnitine C12:0, L-carnitine C16:0, L-carnitine C16:1, and L-carnitine C18:1, were significantly higher in the DCM group than in the control group. Fatty acyl-carnitines are crucial intermediates in the transport of fatty acids into mitochondria for oxidation. The formation of fatty acyl-carnitines allows fatty acid molecules to cross the mitochondrial membrane and enter the mitochondria to be oxidized for energy production [47,48]. This is achieved when a carnitine molecule binds to a fatty acid. The accumulation of long-chain fatty acyl-carnitine and the reduction of short-chain acyl-carnitine in diabetic rats suggest inefficient oxidation of fatty acids by the mitochondria, which could be due to a variety of factors, including insufficient oxygen supply and mitochondria dysfunction [49].

Phospholipids are essential for structure and function of the heart. These molecules play a critical role in many cellular processes, including cell membrane formation, signaling, energy metabolism, and protection against oxidative stress [50–53]. In diabetic rat hearts, we observed significant alterations in the

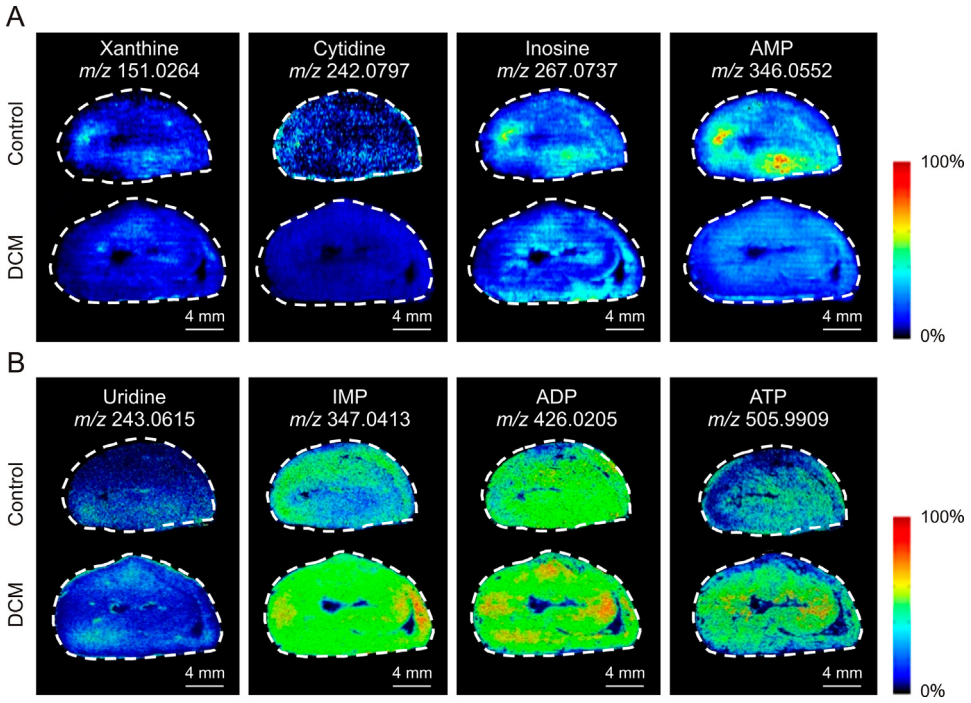

Fig. 8. Ion images of (A) air flow-assisted desorption electrospray ionization (AFADESI)- and (B) matrix-assisted laser desorption ionization (MALDI)-mass spectrometry imaging (MSI) of metabolites involved in nucleotide metabolism in the heart in rats of the control and diabetic cardiomyopathy (DCM) groups. AMP: adenosine monophosphate; IMP: inosine monophosphate; ADP: adenosine diphosphate; ATP: adenosine triphosphate.

localization of PC, PE, PI, phosphatidylglycerol (PG), phosphatidic acid (PA), PS, and sphingomyelin. Our findings demonstrate that PC (34:2) and PC (36:2) were significantly elevated in the myocardium of diabetic rats. The high-resolution MALDI-MSI analysis revealed that these phospholipids show higher abundance in fibrotic lesions than in adjacent normal cardiac tissues (Fig. 5). These findings suggest that changes in the levels of multiple phospholipids may be involved in the pathogenesis of DCM. Although the role of PC in

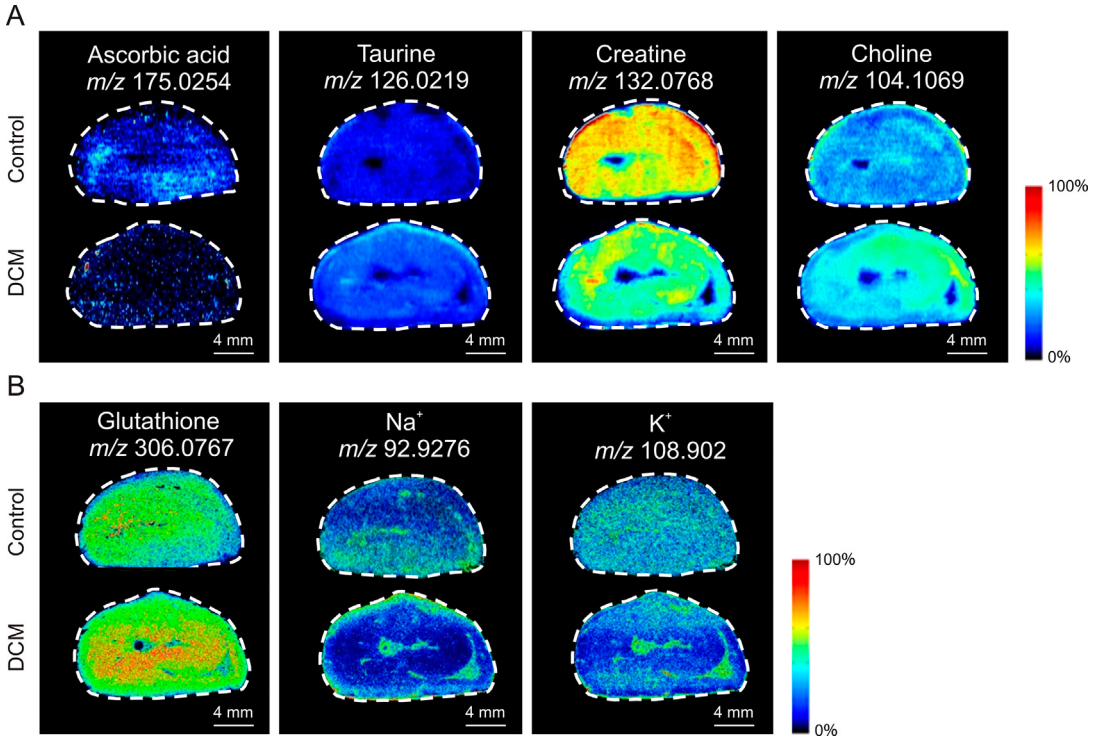

Fig. 9. Ion images of (A) air flow-assisted desorption electrospray ionization (AFADESI)- and (B) matrix-assisted laser desorption ionization (MALDI)-mass spectrometry imaging (MSI) of metabolites involved redox and ion homeostasis in the heart in rats of the control and diabetic cardiomyopathy (DCM) groups.

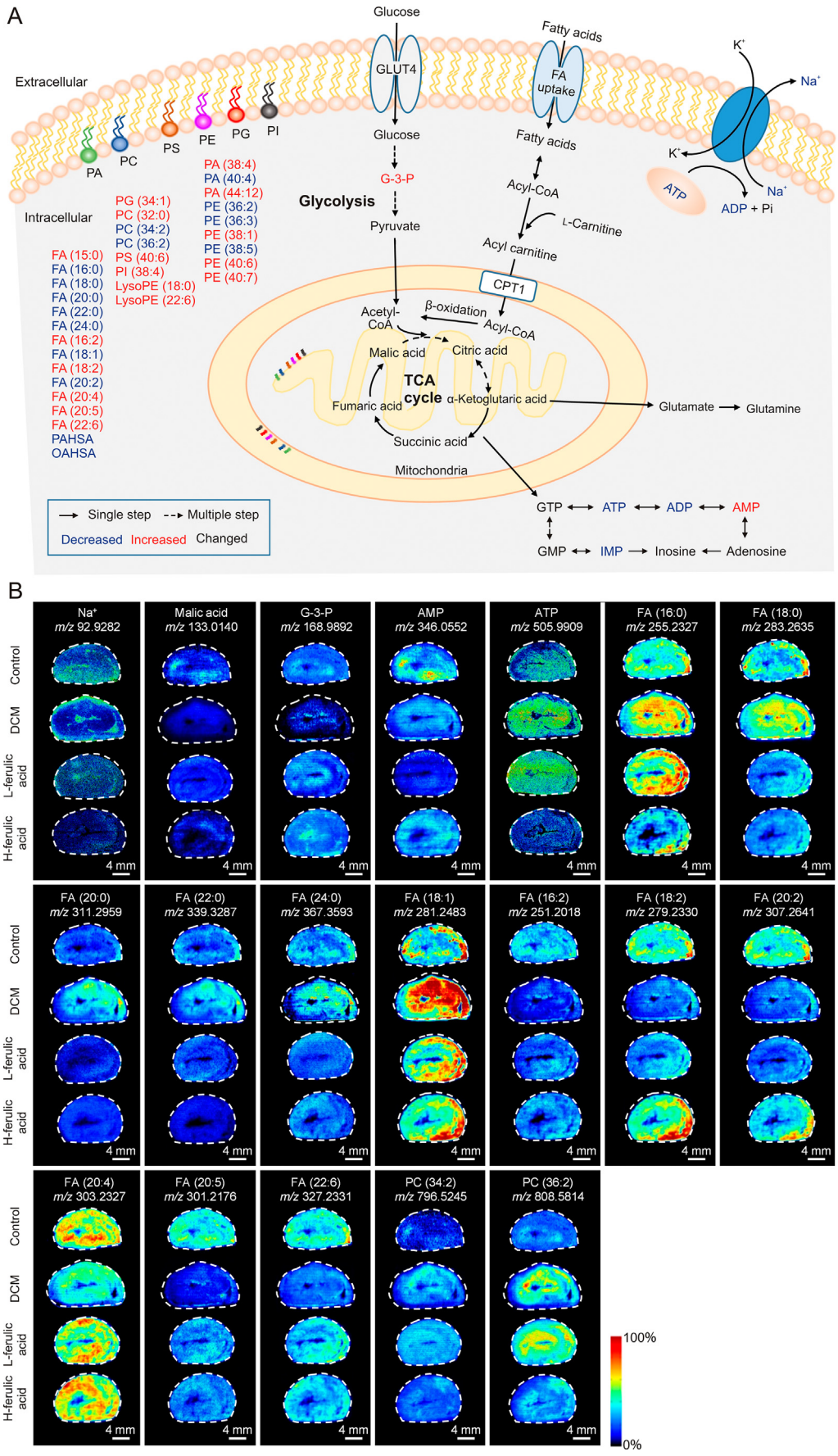
A
Glucose
GLUT4
Glucose
G-3-P
Glycolysis
Pyruvate
Fatty acids
FA uptake
Fatty acids
Acyl-CoA
L-Carnitine
Acyl carnitine
CPT1
Acetyl-CoA
β-oxidation
Acyl-CoA
Malic acid
Citric acid
TCA cycle
Fumaric acid
α-Ketoglutaric acid
Glutamate
Glutamine
Succinic acid
Mitochondria
Extracellular
Intracellular
PA
PC
PS
PE
PG
PI
PA (38:4)
PA (40:4)
PA (44:12)
PE (36:2)
PE (36:3)
PE (38:1)
PE (38:5)
PE (40:6)
PE (40:7)
PG (34:1)
PC (32:0)
PC (34:2)
PC (36:2)
PS (40:6)
PI (38:4)
LysoPE (18:0)
LysoPE (22:6)
FA (15:0)
FA (16:0)
FA (18:0)
FA (20:0)
FA (22:0)
FA (24:0)
FA (16:2)
FA (18:1)
FA (18:2)
FA (20:2)
FA (20:4)
FA (20:5)
FA (22:6)
PAHSA
OAHSA
K+
Na+
ATP
ADP + Pi
GTP ↔ ATP ↔ ADP ↔ AMP
GMP ↔ IMP → Inosine ← Adenosine
Single step
Multiple step
Decreased
Increased
Changed
B
Na+ m/z 92.9282
Malic acid m/z 133.0140
G-3-P m/z 168.9892
AMP m/z 346.0552
ATP m/z 505.9909
FA (16:0) m/z 255.2327
FA (18:0) m/z 283.2635
FA (20:0) m/z 311.2959
FA (22:0) m/z 339.3287
FA (24:0) m/z 367.3593
FA (18:1) m/z 281.2483
FA (16:2) m/z 251.2018
FA (18:2) m/z 279.2330
FA (20:2) m/z 307.2641
FA (20:4) m/z 303.2327
FA (20:5) m/z 301.2176
FA (22:6) m/z 327.2331
PC (34:2) m/z 796.5245
PC (36:2) m/z 808.5814
Control
DCM
L-ferulic acid
H-ferulic acid
4 mm
100%
0%

cardiac fibrosis is not yet fully understood, previous research has linked PC accumulation in fibrotic lesions to increased oxidative stress and inflammation in other organs including the liver and lungs [54,55]. Therefore, it is plausible that similar mechanisms may be involved in the pathogenesis of DCM. Further studies are needed to determine the biological mechanisms by which these phospholipids contribute to DCM.

In the DCM group, we observed significant alterations in the levels and spatial distribution of eight metabolites involved in ATP metabolism (Figs. 8 and S9). In this group, a significant increase in ATP, ADP, IMP, and uridine levels, as well as a significant decrease in AMP, xanthine, cytidine, and inosine levels were detected. Although ATP is a well-known energy molecule, the underlying mechanism that regulates its levels in diabetes has not been fully understood. Elevated ATP levels may initially compensate for metabolic disturbances, but sustained increased levels can lead to detrimental outcomes (e.g., cardiac hypertrophy and fibrosis). AMP, a precursor for ATP and a key regulator of AMP-activated protein kinase (AMPK), plays a crucial role in maintaining energy homeostasis [56,57]. The high-resolution MALDI-MSI analysis revealed that the AMP level in fibrotic diabetic heart tissues was lower than in adjacent normal tissues, suggesting that AMP may be involved in the pathological progression of fibrosis. The significantly lower AMP/ATP ratio in DCM rats than in control rats is associated with increased ATP and decreased AMP levels. This may inhibit AMPK activity, leading to mitochondrial dysfunction, potentially contributing to the occurrence and progression of DCM.

We also observed significant changes in the levels of metabolites involved in oxidative stress (Figs. 9 and S10). Ascorbic acid (vitamin C) and creatine levels were significantly lower in diabetic rats than in the control ones. In contrast, GSH, taurine, and choline levels were significantly higher in the DCM group than in the control group, especially in the myocardium. Ascorbic acid is a potent antioxidant that helps protect cells from oxidative damage, and its decreased levels may contribute to cardiovascular complications in diabetes [58,59]. Creatine is not an antioxidant, but may help reduce oxidative stress and promote cellular energy metabolism by activating CK and recycling ADP [60]. Increased levels of GSH, taurine, and choline levels have not been consistently reported in diabetic hearts. Indeed, some studies have found decreased concentrations of GSH, taurine, and choline can increase oxidative stress in diabetic hearts and contribute to the development of DCM. However, it has been suggested that taurine, GSH, and choline levels may increase in the early stages of diabetes as a compensatory mechanism to counteract excessive oxidative stress [61–63]. The discrepancy between the findings of previous studies suggests that the antioxidant cardiac system is complex, and redox homeostasis can be significantly altered in the diabetic state.

Our study revealed that the levels and distribution of Na^+ and K^+ were significantly altered in the hearts of diabetic rats (Figs. 9 and S10). We found that Na^+ and K^+ levels in the DCM group were higher than in the control group. Several transporters, including Na^+/K^+-ATPase, Na^+-glucose cotransporter, and Na^+-H^+ exchanger, are responsible for maintaining sodium and potassium gradients across the cell membrane [64]. The increased Na^+ and K^+ levels in the hearts of rats in DCM group suggest that hyperglycemia may affect the activity of ion transporters on the cell membrane. The imbalance of ion homeostasis may contribute to cardiac hypertrophy and increase the risk of arrhythmia and heart failure in DCM [65].

3.5. Metabolic regulatory effects of ferulic acid on DCM

Ferulic acid, a natural compound found in various plant-based foods and Chinese herbs, possesses a wide range of pharmacological properties, including anti-inflammatory, antioxidant, anticancer, and vasodilatory activities [66]. Recent studies have demonstrated that ferulic acid has therapeutic potential for treating metabolic syndromes, including diabetes, hyperlipidemia, hypertension, and obesity [67]. We observed that 20 weeks of repeated administration of ferulic acid at a high dose (200 mg/kg) significantly restored the altered levels of metabolites in the hearts of diabetic rats (Figs. 10, S11, and S12). Physiological, biochemical, and histopathological assays confirmed the therapeutic effects of ferulic acid on DCM. Ferulic acid improved energy metabolism by reversing the accumulation of FA (16:0), FA (18:0), FA (20:0), FA (22:0), FA (24:0), and FA (18:1), increasing ATP levels, and reducing G-3-P, malic acid, and AMP levels. Moreover, ferulic acid reversed the inflammatory state of diabetic rat hearts by normalizing the altered levels of multiple lipids, such as FA (16:2), FA (18:2), FA (20:2), FA (20:4), FA (20:5), and FA (22:6). Additionally, ferulic acid may restore ion homeostasis in diabetic rat hearts by reducing Na^+ levels. Interestingly, ferulic acid also exerted anti-fibrotic effects by reducing the accumulation of PC (34:2) and PC (36:2) in fibrotic lesions (Table S7).

The therapeutic effects of ferulic acid on DCM are likely associated with its ability to modulate many cellular processes, including oxidative stress, inflammation, and fibrosis. Ferulic acid can activate AMPK, a key regulator of energy metabolism. AMPK promotes glucose uptake, increases fatty acid oxidation, and stimulates mitochondrial biogenesis, which can improve energy metabolism in various tissues, including the heart [68,69]. Moreover, ferulic acid-mediated AMPK activation may also be associated with anti-inflammatory and antioxidant activities, as it can inhibit the production of pro-inflammatory cytokines and induce the expression of antioxidant enzymes. Furthermore, ferulic acid can modulate the activity of the Na^+/K^+-ATPase, enhancing in cardiac function, reducing in oxidative stress, and preventing myocardial damage in diabetic hearts. Further studies are needed to fully elucidate the underlying cardioprotective effects of ferulic acid and optimize the dosage and treatment duration in clinical settings.

Overall, our results show that ferulic acid exerts its therapeutic effects on DCM by improving energy metabolism, reducing lipotoxicity, regulating inflammatory state, and restoring ion balance.

4. Conclusion

We developed a sensitive, wide-coverage, and high-spatial-resolution MSI approach for mapping metabolites in rat hearts using AFADESI-MSI and MALDI-MSI. Our method successfully identified over 300 metabolites, providing a comprehensive visualization of the metabolic heterogeneity in the heart, metabolic reprogramming in a DCM animal model, and the beneficial effects of ferulic acid on this disease. To our knowledge, this study is the

Fig. 10. Metabolic regulatory effects of ferulic acid on diabetic cardiomyopathy (DCM). (A) Simplified overview of regulation of ferulic acid on metabolic disturbance in DCM. (B) Ion images of air flow-assisted desorption electrospray ionization (AFADESI)- and matrix-assisted laser desorption ionization (MALDI)-mass spectrometry imaging (MSI) of metabolites with significant improvement after ferulic acid treatment. FA: fatty acid; PAHSA: palmitic acid-hydroxystearic acid; OAHSA: oleic acid-hydroxystearic acid; PA: phosphatidic acid; PC: phosphatidylcholine; PS: phosphatidylserine; PE: phosphatidylethanolamine; PG: phosphatidylglycerol; PI: phosphatidylinositol; LysoPE: lysophosphatidylethanolamine; GLUT4: glucose transporter type 4; G-3-P: glyceraldehyde-3-phosphate; Acyl-CoA: acyl-coenzyme A; CPT1: carnitine palmitoyltransferase 1; Acetyl-CoA: acetyl-coenzyme A; TCA: tricarboxylic acid; ATP: adenosine triphosphate; ADP: adenosine diphosphate; GTP: guanosine triphosphate; AMP: adenosine monophosphate; GMP: guanosine monophosphate; IMP: inosine monophosphate; L-ferulic acid: low-dose ferulic acid (50 mg/kg) group; H-ferulic acid: high-dose ferulic acid (200 mg/kg) group.

first to examine the alterations and spatial distribution of endogenous metabolites in the heart under diabetic conditions. We identified over 100 metabolites associated with DCM and revealed their heterogeneous distribution across the heart sections and lesion area. Our findings suggest that region-specific impairments in glucose metabolism, lipid metabolism, nucleotide metabolism, and redox and osmotic homeostasis may contribute to the pathogenesis of DCM. Our results demonstrate that repeated oral administration of 200 mg/kg of ferulic acid for 20 weeks significantly reversed most of these metabolic disorders, especially the alterations in the metabolism of lipids. Our study provides critical insights into the molecular pathology of DCM and the effects of ferulic acid on this disease, highlighting the potential of the AFADESI- and MALDI-MSI approach for applications in heart diseases. The metabolites identified in this study warrant further investigation as potential novel tissue-specific biomarkers for the diagnosis and treatment of DCM.

CRediT author statement

Yanhua Liu: Methodology, Investigation, Visualization, Formal analysis, Writing - Original draft preparation; **Xin Zhang:** Investigation, Formal analysis; **Shu Yang:** Methodology, Resources; **Zhi Zhou:** Methodology; **Lu Tian** and **Wanfang Li:** Investigation; **Jinfeng Wei:** Resources; **Zeper Abliz:** Supervision, Funding acquisition, Writing - Reviewing and Editing; **Zhonghua Wang:** Conceptualization, Investigation, Supervision, Funding acquisition, Writing - Original draft preparation, Reviewing and Editing.

Declaration of competing interest

The authors declare that there are no conflicts of interest.

Acknowledgments

This work was supported by the National Natural Science Foundation of China (Grant Nos.: 21927808 and 81803483).

Appendix A. Supplementary data

Supplementary data to this article can be found online at https://doi.org/10.1016/j.jpha.2023.08.011.

References

[1] J. Bene, K. Hadzsiev, B. Melegh, Role of carnitine and its derivatives in the development and management of type 2 diabetes, Nutr. Diabetes 8 (2018), 8.
[2] G.E. Gilca, G. Stefanescu, O. Badulescu, et al., Diabetic cardiomyopathy: Current approach and potential diagnostic and therapeutic targets, J. Diabetes Res. 2017 (2017), 1310265.
[3] M. Nakamura, J. Sadoshima, Cardiomyopathy in obesity, insulin resistance and diabetes, J. Physiol. 598 (2020) 2977–2993.
[4] M. Tate, D. Prakoso, A.M. Willis, et al., Characterising an alternative murine model of diabetic cardiomyopathy, Front. Physiol. 10 (2019), 1395.
[5] H. Tsutsui, S. Kinugawa, S. Matsushima, Oxidative stress and heart failure, Am. J. Physiol. Heart Circ. Physiol. 301 (2011) H2181–H2190.
[6] W. Li, M. Yao, R. Wang, et al., Profile of cardiac lipid metabolism in STZ-induced diabetic mice, Lipids Health Dis. 17 (2018), 231.
[7] E. Anderson, J.L. Durstine, Physical activity, exercise, and chronic diseases: A brief review, Sports Med. Health Sci. 1 (2019) 3–10.
[8] G.D. Lopaschuk, Q.G. Karwi, R. Tian, et al., Cardiac energy metabolism in heart failure, Circ. Res. 128 (2021) 1487–1513.
[9] C.B. Lietz, E. Gemperline, L. Li, Qualitative and quantitative mass spectrometry imaging of drugs and metabolites, Adv. Drug Deliv. Rev. 65 (2013) 1074–1085.
[10] H. Jiang, Y. Zhang, Z. Liu, et al., Advanced applications of mass spectrometry imaging technology in quality control and safety assessments of traditional Chinese medicines, J. Ethnopharmacol. 284 (2022), 114760.
[11] J.L. Norris, R.M. Caprioli, Analysis of tissue specimens by matrix-assisted laser desorption/ionization imaging mass spectrometry in biological and clinical research, Chem. Rev. 113 (2013) 2309–2342.
[12] R.M. Caprioli, T.B. Farmer, J. Gile, Molecular imaging of biological samples: Localization of peptides and proteins using MALDI-TOF MS, Anal. Chem. 69 (1997) 4751–4760.
[13] K.Y. Garza, C.L. Feider, D.R. Klein, et al., Desorption electrospray ionization mass spectrometry imaging of proteins directly from biological tissue sections, Anal. Chem. 90 (2018) 7785–7789.
[14] Y. Li, B. Shrestha, A. Vertes, Atmospheric pressure molecular imaging by infrared MALDI mass spectrometry, Anal. Chem. 79 (2007) 523–532.
[15] A. Nordström, E. Want, T. Northen, et al., Multiple ionization mass spectrometry strategy used to reveal the complexity of metabolomics, Anal. Chem. 80 (2008) 421–429.
[16] R. Shroff, L. Rulíšek, J. Doubský, et al., Acid-base-driven matrix-assisted mass spectrometry for targeted metabolomics, Proc. Natl. Acad. Sci. U S A 106 (2009) 10092–10096.
[17] T. Müller, S. Oradu, D.R. Ifa, et al., Direct plant tissue analysis and imprint imaging by desorption electrospray ionization mass spectrometry, Anal. Chem. 83 (2011) 5754–5761.
[18] K.A. Douglass, A.R. Venter, Protein analysis by desorption electrospray ionization mass spectrometry and related methods, J. Mass Spectrom. 48 (2013) 553–560.
[19] Y. Zhu, Q. Zang, Z. Luo, et al., An organ-specific metabolite annotation approach for ambient mass spectrometry imaging reveals spatial metabolic alterations of a whole mouse body, Anal. Chem. 94 (2022) 7286–7294.
[20] V.L. Brown, L. He, Current status and future prospects of mass spectrometry imaging of small molecules. Mass Spectrometry Imaging of Small Molecules, Vol. 1203, Humana Press, New York, 2015, pp. 1–7.
[21] R.F. Menger, W.L. Stutts, D.S. Anbukumar, et al., MALDI mass spectrometric imaging of cardiac tissue following myocardial infarction in a rat coronary artery ligation model, Anal. Chem. 84 (2012) 1117–1125.
[22] K. Margulis, Z. Zhou, Q. Fang, et al., Combining desorption electrospray ionization mass spectrometry imaging and machine learning for molecular recognition of myocardial infarction, Anal. Chem. 90 (2018) 12198–12206.
[23] X. Li, J. Wu, F. Xu, et al., Use of ferulic acid in the management of diabetes mellitus and its complications, Molecules 27 (2022), 6010.
[24] S. Anjali, N.P. Padmakumari Soumya, S. Mondal, et al., Cardioprotective effects of ferulic acid in streptozotocin-induced diabetic rats, Bioact. Compd. Heath. Dis. 5 (2022), 149.
[25] L. Ye, P. Hu, L. Feng, et al., Protective effects of ferulic acid on metabolic syndrome: A comprehensive review, Molecules 28 (2022), 281.
[26] H. Liu, R. Chen, J. Wang, et al., 1,5-Diaminonaphthalene hydrochloride assisted laser desorption/ionization mass spectrometry imaging of small molecules in tissues following focal cerebral ischemia, Anal. Chem. 86 (2014) 10114–10121.
[27] M. Huo, Z. Wang, W. Fu, et al., Spatially resolved metabolomics based on air-flow-assisted desorption electrospray ionization-mass spectrometry imaging reveals region-specific metabolic alterations in diabetic encephalopathy, J. Proteome Res. 20 (2021) 3567–3579.
[28] Z. Wang, W. Fu, M. Huo, et al., Spatial-resolved metabolomics reveals tissue-specific metabolic reprogramming in diabetic nephropathy by using mass spectrometry imaging, Acta Pharm. Sin. B 11 (2021) 3665–3677.
[29] D.S. Wishart, Y.D. Feunang, A. Marcu, et al., HMDB 4.0: The human metabolome database for 2018, Nucleic Acids Res. 46 (2018) D608–D617.
[30] C.A. Smith, G. O'Maille, E.J. Want, et al., METLIN: A metabolite mass spectral database, Ther. Drug Monit. 27 (2005) 747–751.
[31] M. Sud, E. Fahy, D. Cotter, et al., LMSD: LIPID MAPS structure database, Nucleic Acids Res. 35 (2007) D527–D532.
[32] P.A. Gorski, D.K. Ceholski, R.J. Hajjar, Altered myocardial calcium cycling and energetics in heart failure: A rational approach for disease treatment, Cell Metab. 21 (2015) 183–194.
[33] D.J. Hamilton, Mechanisms of disease: Is mitochondrial function altered in heart failure? Methodist DeBakey Cardiovasc. J. 9 (2013) 44–48.
[34] S. Alvarez, T. Vico, V. Vanasco, Cardiac dysfunction, mitochondrial architecture, energy production, and inflammatory pathways: Interrelated aspects in endotoxemia and sepsis, Int. J. Biochem. Cell Biol. 81 (2016) 307–314.
[35] L.J. De Meirleir, M. Brivet, A. Garcia-Cazorla, Disorders of pyruvate metabolism and the tricarboxylic acid cycle. Inborn Metabolic Diseases, Springer, Berlin, 2012, pp. 187–200.
[36] P. Rustin, A. Munnich, A. Rötig, Succinate dehydrogenase and human diseases: New insights into a well-known enzyme, Eur. J. Hum. Genet. 10 (2002) 289–291.
[37] K. YuYe, T.O. Yastreb, V. Karpets Yu, et al., Influence of salicylic and succinic acids on antioxidant enzymes activity, heat resistance and productivity of *Panicum miliaceum* L., J. Stress Physiol. Biochem. 7 (2011) 154–163.
[38] H.C. Yoo, Y. Yu, Y. Sung, et al., Glutamine reliance in cell metabolism, Exp. Mol. Med. 52 (2020) 1496–1516.
[39] G. Marazzi, S. Rosanio, G. Caminiti, et al., The role of amino acids in the modulation of cardiac metabolism during ischemia and heart failure, Curr. Pharm. Des. 14 (2008) 2592–2604.
[40] F. Triposkiadis, G. Karayannis, G. Giamouzis, et al., The sympathetic nervous system in heart failure physiology, pathophysiology, and clinical implications, J. Am. Coll. Cardiol. 54 (2009) 1747–1762.
[41] H. Nakamura, S. Matoba, E. Iwai-Kanai, et al., p53 promotes cardiac dysfunction in diabetic mellitus caused by excessive mitochondrial respiration-mediated reactive oxygen species generation and lipid accumulation, Circ. Heart Fail. 5 (2012) 106–115.
[42] L. Salvadó, T. Coll, A.M. Gómez-Foix, et al., Oleate prevents saturated-fatty-acid-induced ER stress, inflammation and insulin resistance in skeletal

muscle cells through an AMPK-dependent mechanism, Diabetologia 56 (2013) 1372–1382.
[43] Y. Wei, D. Wang, F. Topczewski, et al., Saturated fatty acids induce endoplasmic reticulum stress and apoptosis independently of ceramide in liver cells, Am. J. Physiol. Endocrinol. Metab. 291 (2006) E275–E281.
[44] R.S. Khan, A. Chokshi, K. Drosatos, et al., Fish oil selectively improves heart function in a mouse model of lipid-induced cardiomyopathy, J. Cardiovasc. Pharmacol. 61 (2013) 345–354.
[45] L.M. Alaeddine, F. Harb, M. Hamza, et al., Pharmacological regulation of cytochrome P450 metabolites of arachidonic acid attenuates cardiac injury in diabetic rats, Transl. Res. 235 (2021) 85–101.
[46] X. Liu, J. Gao, J. Chen, et al., Identification of metabolic biomarkers in patients with type 2 diabetic coronary heart diseases based on metabolomic approach, Sci. Rep. 6 (2016), 30785.
[47] A. Gnoni, S. Longo, G.V. Gnoni, et al., Carnitine in human muscle bioenergetics: Can carnitine supplementation improve physical exercise? Molecules 25 (2020), 182.
[48] N. Longo, M. Frigeni, M. Pasquali, Carnitine transport and fatty acid oxidation, Biochim. Biophys. Acta 1863 (2016) 2422–2435.
[49] L.A. Calò, E. Pagnin, P.A. Davis, et al., Antioxidant effect of L-carnitine and its short chain esters: Relevance for the protection from oxidative stress related cardiovascular damage, Int. J. Cardiol. 107 (2006) 54–60.
[50] J.N. van der Veen, S. Lingrell, R.P. da Silva, et al., The concentration of phosphatidylethanolamine in mitochondria can modulate ATP production and glucose metabolism in mice, Diabetes 63 (2014) 2620–2630.
[51] X. Yang, J. Liang, L. Ding, et al., Phosphatidylserine synthase regulates cellular homeostasis through distinct metabolic mechanisms, PLoS Genet. 15 (2019), e1008548.
[52] X. Xu, Z. Luo, Y. He, et al., Application of untargeted lipidomics based on UHPLC-high resolution tandem MS analysis to profile the lipid metabolic disturbances in the heart of diabetic cardiomyopathy mice, J. Pharm. Biomed. Anal. 190 (2020), 113525.
[53] A. Vecchini, F. Del Rosso, L. Binaglia, et al., Molecular defects in sarcolemmal glycerophospholipid subclasses in diabetic cardiomyopathy, J. Mol. Cell. Cardiol. 32 (2000) 1061–1074.
[54] E. Ramos-Tovar, P. Muriel, Molecular mechanisms that link oxidative stress, inflammation, and fibrosis in the liver, Antioxidants 9 (2020), 1279.
[55] P. Cheresh, S.J. Kim, S. Tulasiram, et al., Oxidative stress and pulmonary fibrosis, Biochim. Biophys. Acta BBA Mol. Basis Dis. 1832 (2013) 1028–1040.
[56] D.G. Hardie, AMP-activated protein kinase: An energy sensor that regulates all aspects of cell function, Genes Dev. 25 (2011) 1895–1908.
[57] C.L. Lyons, H.M. Roche, Nutritional modulation of AMPK-impact upon metabolic-inflammation, Int. J. Mol. Sci. 19 (2018), 3092.
[58] S. Bhattacharya, Reactive oxygen species and cellular defense system. Free Radicals in Human Health and Disease, Springer, New Delhi, 2015, pp. 17–29.
[59] F.A. Matough, S.B. Budin, Z.A. Hamid, et al., The role of oxidative stress and antioxidants in diabetic complications, Sultan Qaboos Univ. Med. J. 12 (2012) 5–18.
[60] R. Guzun, N. Timohhina, K. Tepp, et al., Systems bioenergetics of creatine kinase networks: Physiological roles of creatine and phosphocreatine in regulation of cardiac cell function, Amino Acids 40 (2011) 1333–1348.
[61] K.S. Kim, D.H. Oh, J.Y. Kim, et al., Taurine ameliorates hyperglycemia and dyslipidemia by reducing insulin resistance and leptin level in Otsuka Long-Evans Tokushima fatty (OLETF) rats with long-term diabetes, Exp. Mol. Med. 44 (2012) 665–673.
[62] H.J. Pan, Y. Lin, Y.E. Chen, et al., Adverse hepatic and cardiac responses to rosiglitazone in a new mouse model of type 2 diabetes: Relation to dysregulated phosphatidylcholine metabolism, Vascul. Pharmacol. 45 (2006) 65–71.
[63] L. Mandelker, Oxidative stress, free radicals, and cellular damage. Studies on Veterinary Medicine, Humana Press, Totowa, 2011, pp. 1–17.
[64] Z. Xu, K.P. Patel, G.J. Rozanski, Metabolic basis of decreased transient outward K^+ current in ventricular myocytes from diabetic rats, Am. J. Physiol. 271 (1996) H2190–H2196.
[65] D.A. Cesario, R. Brar, K. Shivkumar, Alterations in ion channel physiology in diabetic cardiomyopathy, Endocrinol. Metab. Clin. North Am. 35 (2006) 601–610, ix–x.
[66] J.K. Kim, S.U. Park, A recent overview on the biological and pharmacological activities of ferulic acid, Excli J. 18 (2019) 132–138.
[67] Y. Song, T. Wu, Q. Yang, et al., Ferulic acid alleviates the symptoms of diabetes in obese rats, J. Funct. Foods 9 (2014) 141–147.
[68] S. Chowdhury, S. Ghosh, K. Rashid, et al., Deciphering the role of ferulic acid against streptozotocin-induced cellular stress in the cardiac tissue of diabetic rats, Food Chem. Toxicol. 97 (2016) 187–198.
[69] S. Roy, S.K. Metya, S. Sannigrahi, et al., Treatment with ferulic acid to rats with streptozotocin-induced diabetes: Effects on oxidative stress, pro-inflammatory cytokines, and apoptosis in the pancreatic β cell, Endocrine 44 (2013) 369–379.